REAL-TIME MONITORING OF CHEMICAL REACTIONS WITH CARBON NANOTUBE FIELD-EFFECT TRANSISTORS

Heather Elise Wilson

MAY 16, 2014

THESIS ADVISOR: PROFESSOR ETHAN D. MINOT

Table of Contents

1. Abstract

Single-molecule biosensing with carbon nanotube (CNT) field-effect transistors has the potential to reveal important information about chemical and biological kinetics with high spatiotemporal resolution. This method of single-molecule sensing has proven quite challenging to employ. In a search for ways to enhance the practicality of existing protocols, the chemical reaction of diazonium reagents with CNTs in field-effect transistors was explored.

Several experiments were performed in which CNT field-effect transistors were exposed to a diazonium reagent in aqueous solution. The chemical reaction between a diazonium reagent and a CNT resulted in up to a 5-fold increase in the total resistance, R_{total}, of the transistor. Up to a 5-fold reduction in the slope of the sub-threshold region of the transistor curve was also observed. We found that the increase in R_{total} occurred via three separate mechanisms: a decrease in the scattering length of the charge carriers, the presence of scattering "hot spots," and an increase in contact resistance between the CNT and metal electrodes.

The real-time electrical data obtained from the transistor during the CNT and diazonium reaction revealed three notable characteristics. First, periodic, discrete changes in resistance were observed throughout the reaction at differing rates and magnitudes. The source of these discrete changes was unclear. Second, transistors exposed to diazonium reagents showed nearly linear increases in device resistance as a function of reaction time. Third, increasing the gate voltage applied to the CNT channel increased the rate of change in resistance, dR_{total}/dt. We propose that dR_{total}/dt is directly proportional to the rate of bond formation on the CNT sidewall, dN/dt. The predictability of how gate voltage affects dR_{total}/dt allows facile regulation of the reaction rate dN/dt. The ability to control the rate and extent of the diazonium reaction is important for the success of future single-molecule experiments.

2. Introduction

2.1. Background

Biological and chemical sensing with carbon nanotubes (CNTs) is a fascinating area of research that incorporates knowledge across multiple disciplines. There has been much success in the past in measuring the kinetics of biological molecules using other methods [1], [2]. Biosensing with CNTs offers an excellent alternative to traditional methods, with advantages including high sensitivity and the potential for development of hand-held diagnostic devices [3].

The electronic properties of carbon nanotubes are notoriously sensitive to the composition and electrostatic state of their environment [4], which can be a blessing or a curse. The curse of this extreme sensitivity results in relatively unstable transistors for computing applications. However, this extraordinary sensitivity has the potential to be a blessing in the investigation of nano-scale chemical and biological phenomena. The goal of this project is to examine the real-time activity of the enzyme adenylate kinase (ADK) using carbon nanotube field-effect transistors (CNTFETs). The ADK enzyme plays a vital role in the metabolism of living cells as a catalyst in the transference of chemical energy.

A single ADK molecule is approximately 6 nm in diameter, which is about two orders of magnitude smaller than the wavelength of visible light. Single-enzyme kinetics cannot be observed directly as a consequence, but the CNTFET can be used to transduce the nanometer-scale mechanical motions into an electrical signal. Enzymes and other proteins change shape (i.e. conformation) on very short time scales as they operate within a cell. Corresponding movement of the protein's surface charges modify the electric field in the CNT channel, simultaneously effecting alterations in the CNT's conductance [5]. The magnitude and frequency of these conductance fluctuations can reveal important information regarding enzyme kinetics [6].

Fortunately, the Philip G. Collins group at the University of California, Irvine, a well-established research group, has been investigating the use of CNTFETs as single-molecule sensors. The Collins group has successfully observed continuous changes in the conductance of CNTs in the presence of single proteins [5], [6]. The first protein the Collins group explored was lysozyme, a very well-studied enzyme in the biological sciences. The Collins group has published several articles regarding the kinetics of lysozyme and other proteins [3], [6]–[10]. Unfortunately, no other research groups have successfully employed Collins' methods in single-molecule monitoring.

Although repeating this method of monitoring enzyme kinetics has proven challenging, attainment of this goal will provide valuable information to the scientific community. Single-molecule biosensing with CNTFETs has some major advantages when compared with well-established methods such as fluorescence detection, x-ray crystallography and nuclear magnetic resonance (NMR) spectroscopy. Advantages include greater spatiotemporal resolution, very long duration measurements (several hours or more), no need for fluorescent labeling, and the potential for implementation in hand-held diagnostic devices [3]. The present focus in this field of study is to monitor proteins and molecules that have been studied extensively with other instruments to verify the accuracy of CNTFET single-molecule sensing.

2.2. Theory

2.2.1. Carbon nanotube field effect transistor

Carbon nanotubes (CNTs) are composed entirely of carbon atoms arranged in a highly-ordered lattice, with each carbon atom attached to three other carbon atoms at equal angles. CNTs exist in a variety of forms with varying electrical characteristics [11]. Conceptually, a CNT can be thought of as a sheet of graphene rolled into a tube. The angle at which the sheet is rolled largely determines whether the resulting CNT will be metallic or semiconducting. As illustrated in Fig. 2.1, there are many angles at which a sheet of graphene can be rolled, but there are three basic configurations: armchair, zigzag and chiral. The armchair configuration is always metallic, the zigzag and many possible chiral forms can be semiconducting, quasi-metallic or metallic.

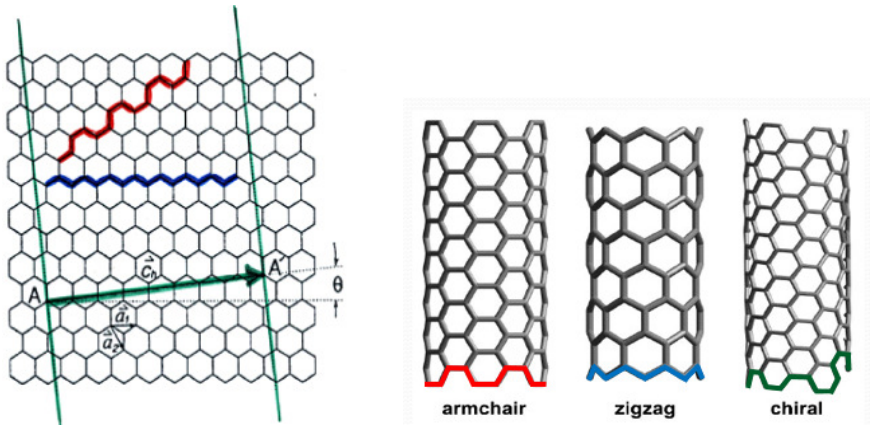

Figure 2.1: Illustration of the various ways a carbon nanotube can be "rolled up" from a graphene sheet. The red line outlines the end of an armchair CNT, the blue line outlines the end of a zigzag CNT. The green arrow represents the angle at which a chiral CNT could be oriented. Source: Scarselli et al. J. Phys.: Condens. Matter 2012 [11].

The nanometer-scale size of semiconducting CNTs makes them excellent candidates for use in quasi-one-dimensional transistors. The CNT serves as the transistor channel. The conductance of the CNT (where conductance is $G \equiv 1/R = I_{sd}/V_{sd}$) can be controlled by applying an electric field of varying polarity and strength. The Minot group works with both ambipolar (small band-gap) and p-type (large band-gap) CNT field-effect transistors (CNTFETs), whose geometry is shown in Fig. 2.2a. For biosensing purposes, applying a voltage to the liquid is the most efficient way to generate an electric field at the CNT channel. This method is referred to as liquid-gating.

In a large band-gap CNT, the charge carriers are positively charged holes. When a positive voltage is applied relative to the CNT channel, an electric field is generated that drives the positively charged holes out of the channel. As a result of the decrease in positive charge carrier concentration, the conductance of the CNT is reduced. The device turns off when a sufficiently large positive voltage is applied. When the voltage applied to the liquid is negative with respect to the channel, electrons are driven out of the channel, which increases the concentration of holes. The conductance of the CNT then increases until a maximum conductance is reached. A sample transistor curve acquired from a CNTFET with a large band-gap CNT is shown in Fig. 2.2b.

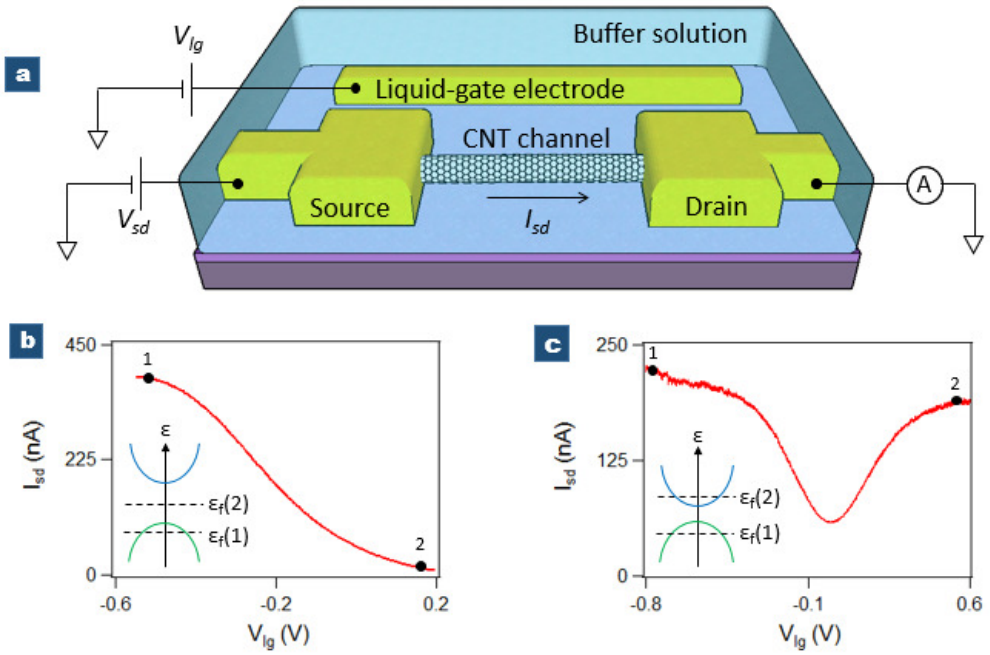

Figure 2.2: a) CNTFET device geometry under liquid. b) Sample transistor curve from a large band-gap and c) small band-gap device, gated in liquid. Insets show the Fermi energy level ε_f at the points indicated on the transistor curves, relative to the valence (green) and conduction (blue) energy bands. The horizontal axis of the band diagram is the charge carriers' wave vector k.

A quasi-metallic CNT has a small band-gap and is capable of conducting both holes and electrons, depending on the gate voltage applied. Figure 2.2c displays a transistor curve from a small band-gap device. A quasi-metallic device typically does not turn off at room temperature. The resulting transistor curve has nearly zero slope for very negative and very positive V_{lg}, with a dip in conductance somewhere in between.

To explain quasi-metallic CNT behavior, the energy band structure of the electrons in the CNT must be considered. Due to their wave-like nature, electrons bound to an atomic lattice must have quantized energies. The electrons can exist in the valence energy band or the conduction energy band. The difference in energy between these bands is called the energy band-gap, ε_g. The energy value below which all energy states are occupied is called the Fermi level ε_F, or total chemical potential μ, of a system. No states are occupied above ε_F by definition. Applying a gate voltage to a CNTFET causes the Fermi level to shift. When ε_F resides above the conduction band, electrons are the charge carriers. When ε_F is below the valence band, holes are the charge carriers. When the Fermi level is in the middle of a small band gap, conduction is at a minimum and propagates via thermally generated electron-hole pairs [12]. The gate voltage for which minimum conduction occurs is called the charge neutrality point. For a CNT with a large band gap, conduction is reduced to zero when ε_F is in the band gap due to insufficient thermal energy at room temperature.

When the gate voltage of a CNTFET is held constant, the resistance of the CNT can be described simply by the linear equation $R(L) = \rho L + R_c$, where ρ is the 1-dimensional resistivity (resistance per unit length) of the CNT, and R_c is the metal-to-CNT contact resistance [13]. At room temperature, a pristine CNT has a resistivity of about $\rho \cong 8\ k\Omega/\mu m$, and a pair of perfectly Ohmic contacts adds a quantum of resistance, $R_c = h/(4e^2) \cong 6.5\ k\Omega$ [13]. (The factor of 4 in the resistance quantum is due to the existence of 4 conduction channels in the CNT: 2 from electron spin, and 2 from band degeneracy.)

The resistivity of a material depends on the material's charge carrier density, velocity and scattering time. These effects can be explained using the Free Electron Model (also called the Drude-Sommerfeld model) [14]. Although this model is based on incorrect assumptions, a more rigorous derivation yields the same results and can be applied to the CNT and most systems of interest. Resistivity is given by

$$\rho = \frac{m}{ne^2\tau} = \frac{v_F m}{ne^2 l}$$

where m is the effective mass of the charge carrier, ne is the 1D charge carrier density, τ is the average time between scattering events, v_F is the charge carrier's average velocity, and l is the mean free path

of the electron. The effective mass of a charge carrier is determined by band-structure computations. The charge carrier's velocity is related to τ and l by $v_F = l/\tau$. Electron scattering events are caused by collisions with phonons (thermal lattice vibrations), as well as impurities and lattice defects. Computational studies have found that individual lattice impurities and defects increase the resistance of a CNT by a quantity on the order of a quantum unit of resistance, $h/(2e^2)$ [15].

2.2.2. Single-molecule sensing with a CNTFET

Proteins are composed primarily of amino acids. Some of the amino acids residing on the surface of the protein have charged atoms. Many enzymes, including lysozyme and adenylate kinase, change shape as they act on their target molecule (the substrate). Generally, the shape changes (i.e. conformational transitions) tend to occur as an opening and closing of the molecule. The open and closed states of ADK are shown in Fig. 2.3a. As the conformational changes occur, the charged surface atoms move with the rest of the protein.

When a protein is attached to CNT as shown in Fig. 2.3b, these charged atoms approach or recede from the CNT, altering the electric field at the CNT channel. The electric field alterations cause a change in the conductance of the device, which can be observed as a change in current between the source and drain electrodes. A sample data set from the Collins group illustrating this concept is displayed in Fig. 2.3c.

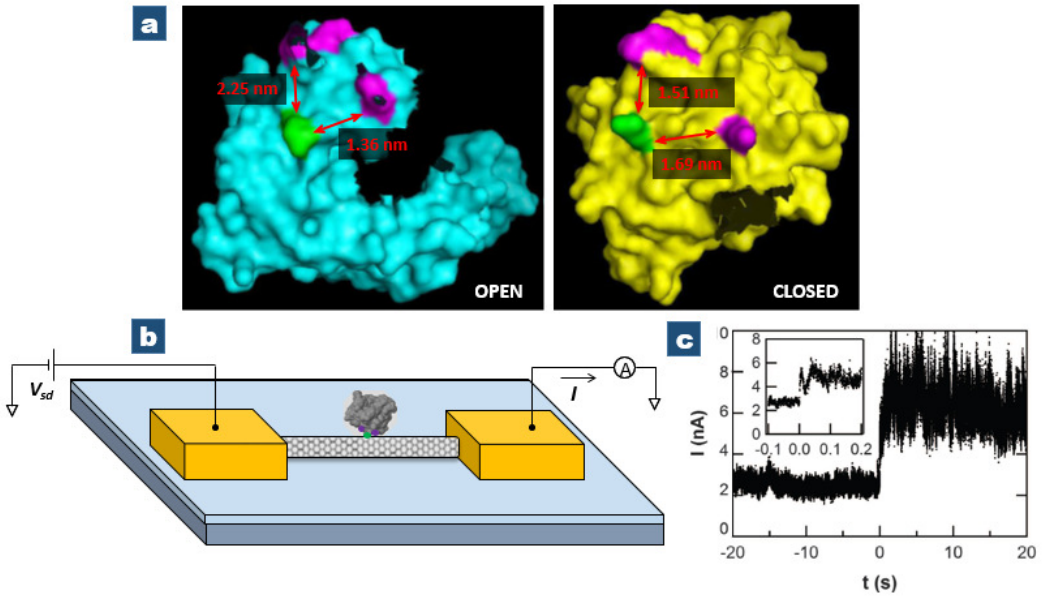

Figure 2.3: a) Open and closed conformations of adenylate kinase (Source: www.pdb.org, files 1AKE and 4AKE). The CNT attachment site is highlighted in green, neighboring charged amino acids in purple. b) A single ADK enzyme attached to the CNT channel and c) a sample data set [9] showing that a signal is observed when the protein is exposed to substrate at t = 0 s.

Some debate exists regarding what mechanism causes the conductance changes in response to protein movement. The Collins group proposes that the protein surface charges act effectively as an electrostatic gate [5], [9], see Fig. 2.4b. The competing theory suggests that the protein surface charges act as a potential well or potential barrier depending on the sign of the surface charge(s) [16], see Fig. 2.4c.

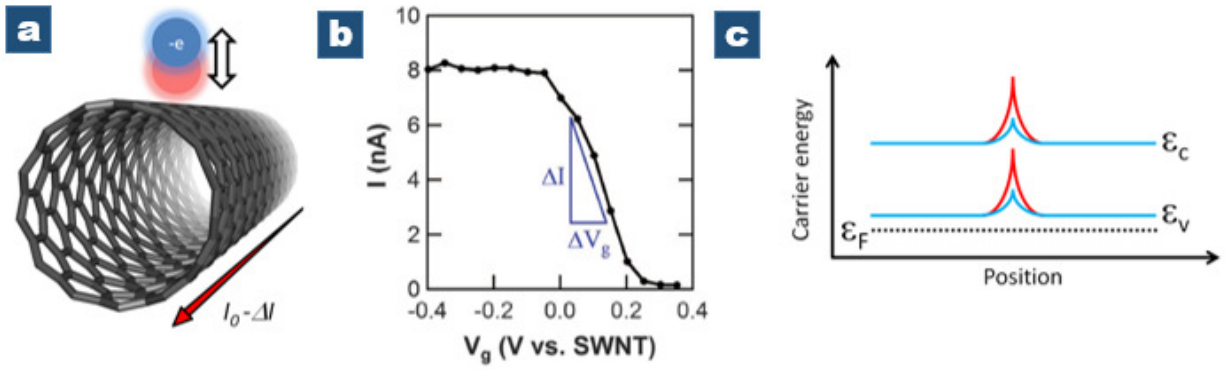

Figure 2.4. a) Representation of a protein surface charge changing position with respect to the CNT. b) Transistor curve with inset proposing that charge movement effectively alters the gate voltage experienced by the CNT by ΔV_g [9]. c) Qualitative diagram suggesting that protein surface charge movement alters the height of the potential barrier at the protein's position on the CNT. The blue line represents the barrier caused by a positive charge far from the p-type CNT, and red line depicts the barrier for a positive charge near the CNT.

There exists a way to determine which mechanism is responsible for the conductance changes. In the potential barrier scheme, the magnitude of the conductance changes have a strong dependence on the sign of nearby charges. The charge carriers in the CNT are positively charged holes, therefore a neighboring positive charge will act as a barrier and scatters the holes strongly. A nearby negative charge creates a potential well, and scatters holes more weakly. In the effective gating scheme, the sign of the proximate charge does not affect the magnitude of the conductance changes, only the sign of ΔI is affected. The Minot group is presently investigating this question.

2.2.3 Bioconjugation chemistry

This project necessitates determination of an effective way to attach a single ADK enzyme to a CNT. Fortunately, the Minot Research Group has some experience in this regard. Graduate student Tal Sharf in the Minot group is using pyrene maleimide molecules as a way to link proteins to CNTs. The pyrene forms a strong non-covalent bond with the CNT, while the maleimide substituent forms a covalent bond with the thiol group of a cysteine amino acid on the surface of the protein. The protein is engineered so

that the cysteine residue expresses at a location far from the active site of the protein [6]. Fig. 2.5a shows how the cysteine mutant can be used to attach the ADK protein to a CNT. Graduate student Hiral Patel was using a protein with a hydrophobic tail that can easily adhere to the CNT without the need of an additional linker molecule. The Minot group has not determined which method is best, and the answer to this question may depend on the type of protein being studied.

Another alternative for bioconjugation is being considered: Dr. Landon Prisbrey, a former post-doctoral researcher in the Minot group, initiated investigations of the chemical reaction between CNTs and carboxybenzene diazonium salt (CBD). The carboxybenzene groups formed on the CNT [17] can be used to covalently attach proteins [18], [19] as shown in Fig. 2.5b. Dr. Prisbrey conducted experiments in which he exposed a single CNT in a CNTFET to an aqueous solution of CBD while simultaneously monitoring the CNT's conductance. The data he obtained showed interesting characteristics of the reaction that were not yet fully understood. Continuation of Dr. Prisbrey's work may enable determination of the approximate number of protein attachment points created on the CNT, and how these points impact the CNT's electronic behavior. These attachment points form defects in the lattice of the CNT. Defects can alter the CNT's electrostatic responses to nearby charges (e.g. surface charges on enzymes), as well as alter the CNT's charge transport characteristics [20], [21].

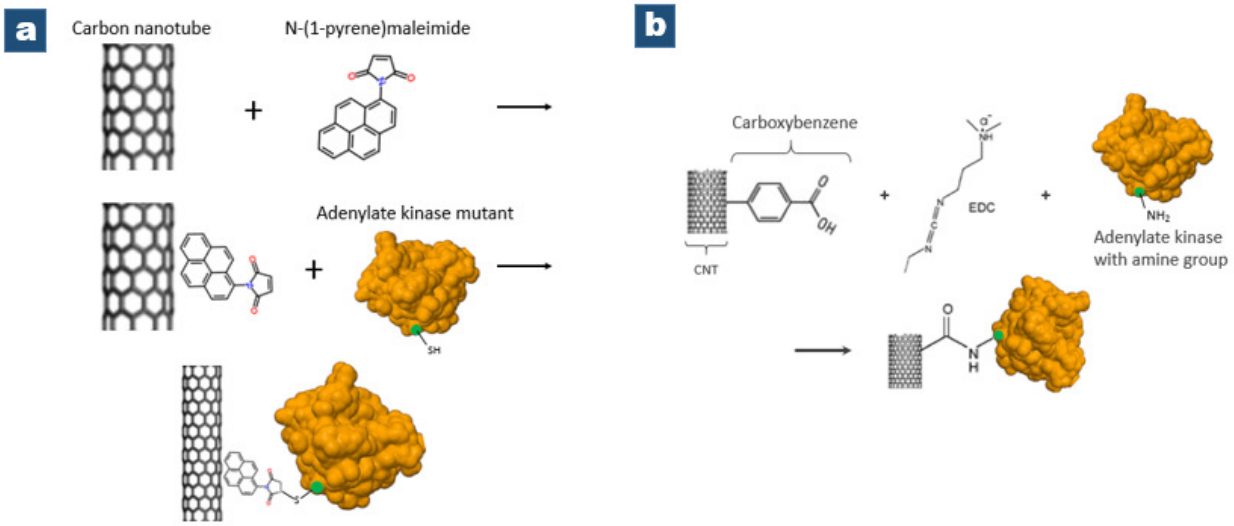

Figure 2.6. Possible protein attachment schemes: a) chemical reaction showing how a pyrene maleimide linker molecule can be used to attach adenylate kinase to a CNT, and b) chemical reaction scheme showing how carboxybenzene defects can be used to covalently attach proteins [18]. Source: protein image from www.pdb.org, file 1AKE.

2.2.4 Diazonium chemistry

It is helpful to discuss the details of the chemical reaction between diazonium reagents and carbon nanotubes, as that is the focus of the results of this thesis. This chemical reaction has been investigated and discussed extensively in literature [22]–[26]. Figure 2.7a shows the general structure of a diazonium reagent, as well as the specific diazonium compounds investigated in this work.

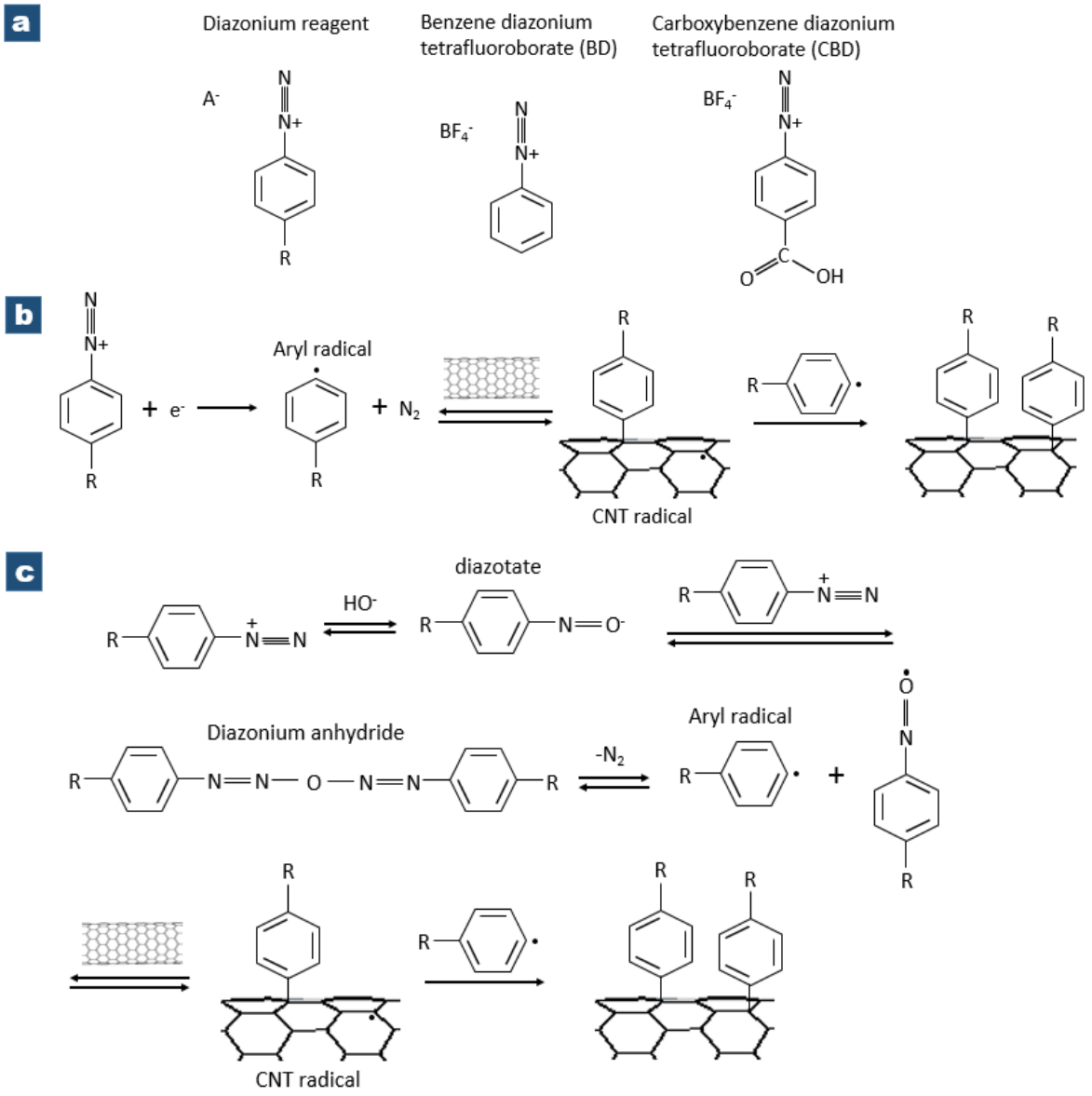

Figure 2.7. a) The general form of a diazonium reagent is any anion and a cation with two triply bonded nitrogen atoms attached to a benzene ring. (The R represents any organic side group.) Carboxybenzene diazonium and benzene diazonium tetrafluoroborate were used in this study. b) - c) The reaction of diazonium reagents with a CNT can occur via two different mechanisms.

There are primarily two different reaction schemes proposed for the formation of carboxybenzene groups on CNTs. The scheme in Fig. 2.7b is the most commonly referenced, in which an electron reduces the cation of a diazonium salt to an aryl radical and nitrogen gas. The aryl radical then forms a bond with the CNT. The second reaction scheme differs from the first in regards to the formation of the aryl radical, as shown in Fig. 2.7c. In this alternative reaction scheme, a hydroxide ion in solution initiates the conversion of a diazonium cation to diazonium anhydride, which then dissociates into an aryl radical and diazo-radical. The second reaction scheme is favored at high pH [24].

The newly formed aryl radicals are highly reactive. A radical is a molecule (usually neutral in charge) with an unpaired electron. The unpaired electron causes the molecule to be very unstable, and tends to form bonds by pairing up with electrons on other molecules [27]. When an aryl radical forms a bond with the CNT, the CNT then becomes an unstable radical itself. Depending the degree of instability and proximity of other aryl radicals, the newly attached aryl group on the CNT may desorb, or a second CNT-aryl bond may be formed.

A recent computational study suggested that smaller diameter CNTs form more stable bonds with aryl radicals due to relief of angular strain in the CNT [28]. The angular strain is caused by the cylindrical shape of the CNT, which bends the carbon bonds out of their normally planar configuration. The planar shape results from partial hybridization (sp^2) of the electron orbitals, as shown in Fig. 2.8. The single electron in the unhybridized p_z orbital is conductive. When the CNT forms a new bond, the bonding carbon becomes sp^3 hybridized and "puckers" into a tetrahedral shape, thus relieving the angular strain.

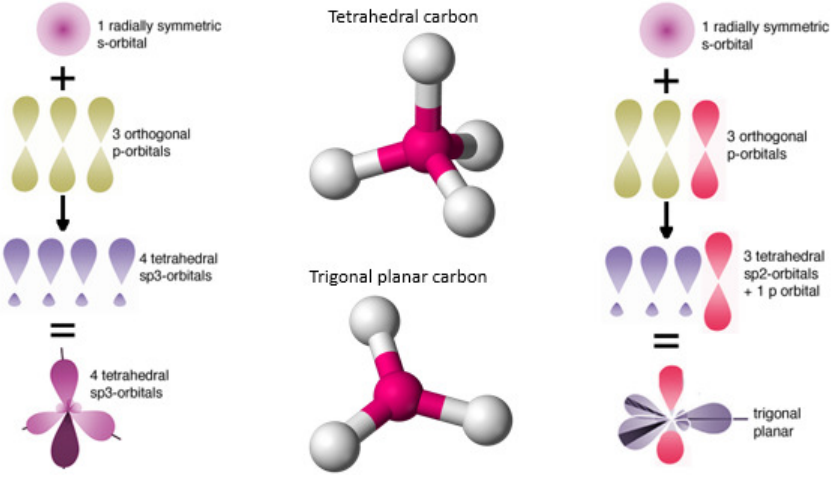

Figure 2.8. Carbon atoms participating in bonds have hybridized s (l = 0) and p (l = 1) orbitals. Pristine CNT carbon atoms are sp^2 hybridized, and become sp^3 hybridized after bonding to an aryl group. Source: http://besocratic.colorado.edu/CLUE-Chemistry/chapters/chapter3txt-3.html.

3. Methods

3.1. Summary

To perform single-molecule experiments, the carbon nanotube field-effect transistors (CNTFETs) were fabricated in the Minot lab. After fabrication, lysozyme was attached to the CNT in the CNTFET. Attaching a single molecule at a precise orientation cannot be done mechanically because of the molecule's smallness, so a chemical "self-assembly" method was utilized instead. Once the CNTFET had been functionalized with lysozyme, electrical measurements were taken of the CNTFET prior to and after administration of the lysozyme substrate.

3.2. Preparation of carbon nanotube field-effect transistors

3.2.1. Photolithography

Carbon nanotube field-effect transistors (CNTFETs) were fabricated in-house in the Minot lab using standard photolithographic and metal deposition techniques. The general device fabrication scheme is shown below in Fig. 3.1. The carbon nanotubes (CNTs) were grown by chemical vapor deposition (CVD) and gold electrodes were patterned on top of the CNTs.

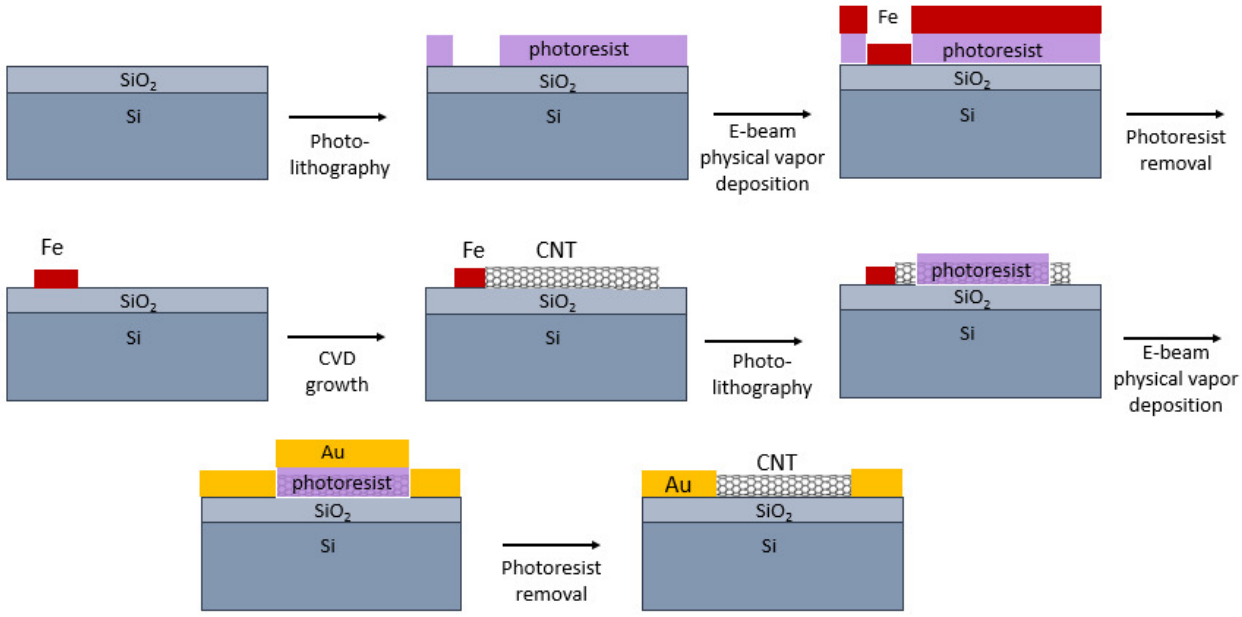

Figure 3.1. Step-by-step CNTFET fabrication scheme. Iron catalyst pads were patterned onto silicon wafers using photolithography "stenciling," then CNTs were grown by chemical vapor deposition. Gold electrodes and contact pads were patterned over the CNTs using photolithography.

A silicon wafer with a 500 nm layer of thermally-grown oxide (Nova Electronic Materials) served as the base of the CNTFET devices. To begin the photolithography process, the silicon wafer was dehydrated on a hotplate at 190°C for 1 minute. A layer of P20 primer was spin-coated on at 4000 rpm for 30 seconds to improve adhesion of subsequent layers. Next, LOR3A photoresist (Microchem) was spun on at 4000 rpm for 45 seconds, and then baked for 4 minutes on a hot plate at 190°C. This first layer of photoresist ensures the desired contour of edges after lift-off of the developed photoresist. A layer of Shipley 1813 photoresist was then spun on at 4000 rpm for 30 seconds. The wafer was then baked at 115°C for 90 seconds.

An optically transparent mask with a patterned coating of chrome was placed on top of the wafer. The pattern used in the first step of the fabrication process was the pattern for the catalyst pads. The wafer with mask on top was then exposed to 350 W near-UV (365 nm to 405 nm) light for 5 seconds. The wafer was then washed in AZ726 MIF developer for 90 seconds to remove the exposed portions of the photoresist layer.

3.2.2. Electron beam physical vapor deposition

Iron catalyst was then deposited onto the photoresist "stencil". The electron-beam physical vapor deposition system was used to deposit approximately 35 nm of SiO_2, and then 1 nm of iron. The SiO_2 provides a porous base for iron nanoparticles to form, which is desired for CNT growth. After deposition, the wafer was soaked overnight at 70°C in Remover PG to remove the photoresist and attached SiO_2 and Fe. The areas without photoresist retain the materials deposited by the electron beam system.

3.2.3. Chemical vapor deposition

The wafer was then ready for CNT growth via chemical vapor deposition. The iron-patterned wafer was inserted into a 4-inch quartz-tube furnace. The wafer was baked in open-air at 600°C for 5 minutes to remove any residual organic materials. Then, with the furnace sealed, the wafer was heated to 900°C under H_2 gas at a flow rate of 0.45 SLM (standard liters per minute). The temperature was held at 900°C for 5 minutes while 0.3 SLM methanol vapor and 0.15 SLM ethanol vapor were bubbled into the furnace with argon gas, in addition to the 0.45 SLM H_2 gas. The methanol and ethanol provide a source of carbon for CNT formation, while the hydrogen gas reduces the iron to optimize CNT growth.

Once the CNTs had been grown on the wafer, the gold electrodes were deposited. The photolithography and electron beam physical vapor deposition processes were repeated as described above. For the

deposition, approximately 1 nm Ti was deposited as an adhesive layer, followed by approximately 50 nm Au.

3.3. Attachment of lysozyme to CNT

Self-assembly with bulk chemistry was used to attach the lysozyme to a CNT. The protocol used for attaching lysozyme was initially developed by Collins [9]. An illustration of the general scheme is shown in Fig. 3.2. The following description includes some additional details and minor modifications from the Collins protocol.

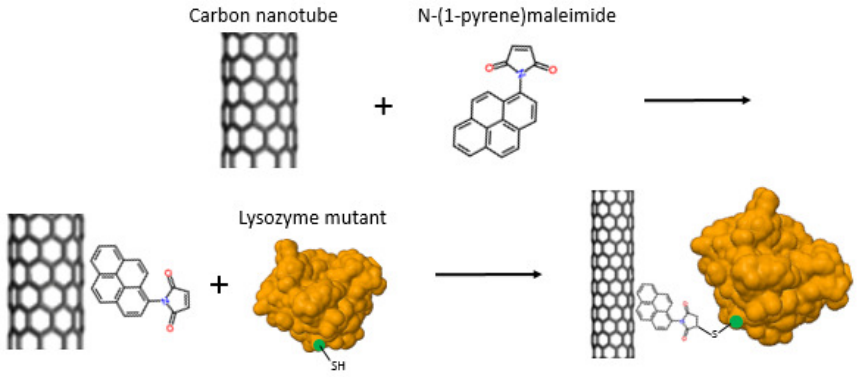

Figure 3.2. Illustration showing how the lysozyme was attached to a carbon nanotube. The four benzene rings (pyrene) of the pyrene maleimide adhere non-covalently to the CNT, and the maleimide part forms a covalent bond with the cysteine residue on the lysozyme.

First, a piece of plastic paraffin film (brand name Parafilm) was cut into a rectangular window shape and applied to the CNTFET device. The purpose of the window was to contain a bubble of fluid for protein incubation and electrical measurements, with CNTs in the middle of the window. The chip with the Parafilm was then baked at 115°C for 2 minutes to improve adhesion.

A solution of 1 mM pyrene maleimide in ethanol was prepared by adding 3 mg of pyrene maleimide to 10 mL of ethanol. The solution was then sonicated for 2 minutes. The CNTFET was soaked in the pyrene maleimide solution for 30 minutes without agitation. The pyrene maleimide acts as an adhesive for the lysozyme, where the group of benzene rings on the pyrene maleimide form a non-covalent bond with the CNT, and the maleimide portion of the molecule forms a covalent bond with an engineered cysteine residue on the lysozyme.

To remove excess pyrene, the CNTFET undergoes a series of washes prior to incubation with lysozyme. A solution of 0.1% Tween-20 in ethanol was prepared by adding 40 µL of Tween-20 to 40 mL of deionized

water (DI H_2O). The solution was mixed with a magnetic stir bar at 500 rpm for 5 minutes. The solution must be mixed thoroughly and prepared immediately prior to use for desired results.

The CNTFET was washed in the 0.1% Tween-20 solution on an orbital shaker at 110 rpm for 30 minutes. A second wash was done in a solution of half 0.1% Tween-20 in ethanol and half 20 mM phosphate buffer (pH 7.2) for 10 min on the orbital shaker at 110 rpm. The CNTFET was then rinsed in DI H_2O on the orbital shaker for 5 minutes at 110 rpm.

The S90C lysozyme mutant used in the next step was synthesized by the Unnatural Protein Facility at OSU. The S90C mutation designation indicates that the 90th amino acid in the lysozyme sequence, which is normally serine (S), was replaced with cysteine (C). The location of the mutation was selected to ensure the observation of a large signal during the biosensing experiment. An EnzChek Lysozyme Assay was used to confirm that the activity rates of the mutant and wild type proteins were very similar, see Fig. 3.3. Collins also reported that the structure and activity of the protein was unaltered by this mutation [6], [10].

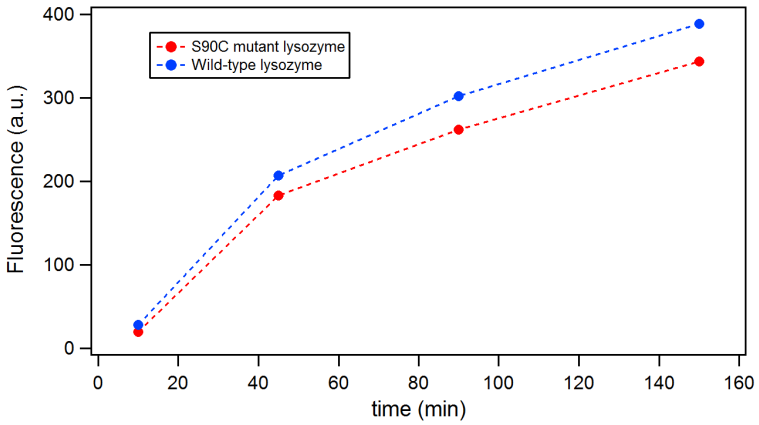

Figure 3.3. Results of fluorescence assay comparing the activity of wild-type lysozyme and S90C mutant lysozyme, 0.5 mg/mL each, upon exposure to substrate (*Micrococcus lysodeikticus*) labeled with fluorescein. Fluorescence measured is proportional to mass of substrate consumed.

To attach the lysozyme to the CNT, a solution of T4 lysozyme S90C mutant was prepared by diluting a concentrated stock solution with 20 mM phosphate buffer (pH 7.2) to yield a 54 µM solution. A bubble of the lysozyme solution was applied to the surface of the CNTFET and allowed to incubate (soak) for 60 minutes without agitation.

Excess, unreacted protein was then removed. A wash buffer consisting of 10 mM phosphate buffer, 5 mM KCl and 0.05% Tween-20 at pH 7.2 was prepared a few minutes prior to the end of the incubation

period. The Tween-20 was added to the buffer-salt solution and stirred at 500 rpm with a magnetic stir bar for 5 minutes. The CNTFET was washed on the orbital shaker at 110 rpm for 30 minutes using the freshly prepared wash buffer to remove unreacted lysozyme. The CNTFET was then washed in DI H_2O on the orbital shaker at 110 rpm for 5 minutes.

Finally, the functionalized CNTFET was submerged in a phosphate-buffered saline (PBS) solution. The lysozyme remained in PBS without drying until completion of experiments. The functionalized CNTFET underwent electrical measurements within 24 hours of protein attachment. Collins reports that devices can be refrigerated and stored in PBS for up to two weeks without loss of activity [6], [10].

To check the success and density of lysozyme attachment, an Asylum MFP3D atomic force microscope (AFM) was used to generate images of the CNT before and after performing the procedure described above. Approximately 4 µm x 4 µm images were obtained with the AFM operated in attractive tapping mode. The images were acquired on a dry CNTFET, after completion of electrical measurements.

3.4. Electrical measurements

A semiconductor probe station equipped with tungsten needles for contacting the gold pads was used for the electrical measurements. A circuit diagram is shown in Fig. 3.4 illustrating the connections made to the CNTFET, as well as corresponding example measurements. The active portion of the CNTFET was submerged in a bubble of buffer solution, contained by the Parafilm window described previously. A Yokogawa GS200 DC Voltage/Current Source device was used as the voltage source for the liquid-gate electrode (V_{lg}). A Stanford Research Systems Low-Noise Current Preamplifier SR570 was used to measure the source to drain current (I_{sd}) and also to supply the source electrode voltage (V_{sd}). A National Instruments M-Series DAQ was used to convert the analog signal from the preamplifier to a digital signal. The signal was collected and displayed by a homemade LabVIEW computer program.

A 25 mV source-drain bias, V_{sd}, was applied to the device. To begin, a measurement of the Faradaic current, $I_{Faradaic}$, was obtained. Faradaic current is the current generated by electron transfer from a metal to an electrolyte. The Faradaic current increases exponentially beyond a threshold value. This electrochemical current was avoided in these experiments, only the current that flows through the CNT from source to drain, I_{sd}, was desired. To determine the exact range of minimal Faradaic current, the source probe needle was disconnected while a range of values for the liquid gate potential was swept. CNTFETs were operated within the acceptable range, defined as $I_{Faradaic} < 1$ nA. For most of our devices, this range was approximately -800 mV < V_{lg} < +400 mV.

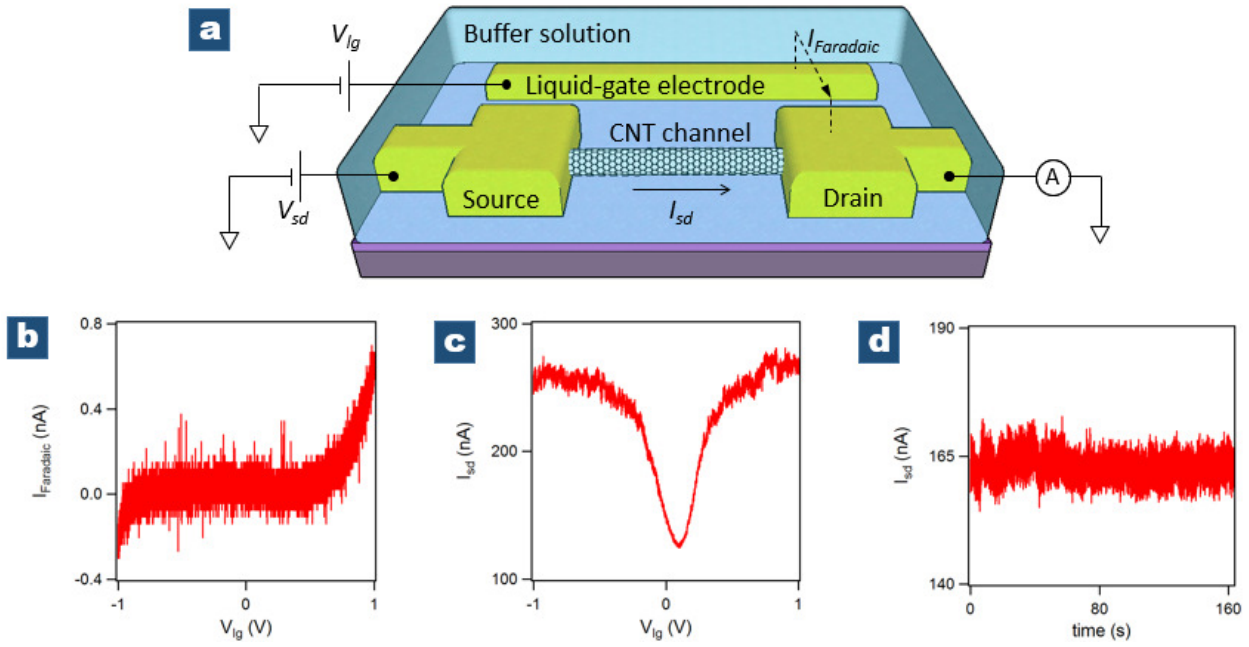

Figure 3.4. a) CNTFET submerged in an aqueous buffer solution and sample data sets of: b) Faradaic current measurement, c) transistor curve measurement, and d) recording of current in CNT as a function of time (constant V_{lg}).

For the single-molecule biosensing experiments, the source probe needle was reengaged and the liquid gate electrode was held at a constant potential. Phosphate-buffered saline (PBS) at pH 7.0 to 7.5 was the buffer solution used. The potential chosen was such that the CNTFET was approximately half-way between the on and off states (or minimum and maximum current in a small band-gap device). The preamplifier filtering was turned off, and the gain was set to high-bandwidth mode. The sensitivity of the preamplifier was set to 100 nA/V, where the output of the preamplifier ranges from 0.0000 V to 6.000 V. The current was monitored at a 20,000 samples per second. The background current prior to the addition of the substrate was observed and recorded for comparison to biosensing data.

The substrate administered to the lysozyme was peptidoglycan. A 2.5 mg/mL solution of peptidoglycan in PBS was prepared. Approximately 2/3 of the PBS solution in the Parafilm window reservoir was replaced with the peptidoglycan solution via pipette. The current through the CNTFET, I_{sd}, was monitored for up to 30 minutes after the addition of substrate. Instrument settings during this period were the same as described for the background measurements.

For the diazonium experiments, 20 mM 2-(N-morpholino)ethanesulfonic acid (MES) buffer at pH 4.5 to 4.6 was used. The diazonium reagents benzene diazonium (BD) and carboxybenzene diazonium (CBD)

were previously synthesized by Professor Daniel Myles, and stored at -20^{o}C until ready for use. Enough solid diazonium reagent was gently mixed into 20 mM MES buffer to make approximately 3 mL of 1.5 mM to 60 mM BD or CBD. The diazonium solution was prepared approximately 5 minutes prior to applying to a CNTFET. A Parafilm window was also used in these experiments. The solution in the Parafilm window was exchanged via pipette to the diazonium solution while $I_{sd}(t)$ was simultaneously recorded at 6000 samples per second. Exposure time of the CNTFETs to the diazonium solution varied from 20 minutes to 2 hours. The liquid gate voltage V_{lg} was modified during exposure in many cases (see Results section).

4. Results

Several experiments were conducted in which a CNTFET was exposed to a solution of carboxybenzene diazonium (CBD) or benzene diazonium (BD). The source-drain current, I_{sd}, of the CNTFET was monitored before, during and after exposure. Experimental conditions, including chemical species, liquid-gate voltage and source-drain voltage, were varied. The rates of change in the resistance of the CNTFETs were compared under different conditions. The diameters of the CNTs before and after diazonium exposure were also compared.

Following exposure to CBD or BD, all devices displayed an overall decrease in conductance. Transistor curves of the CNTFETs were acquired before and after diazonium exposure, representative examples are shown in Fig. 1. In addition to an overall decrease in conductance, a shift in the charge neutrality point (CNP) to a more positive gate voltage was observed in all cases. The slope of the transistor curve between the on-state and off-state decreased as well.

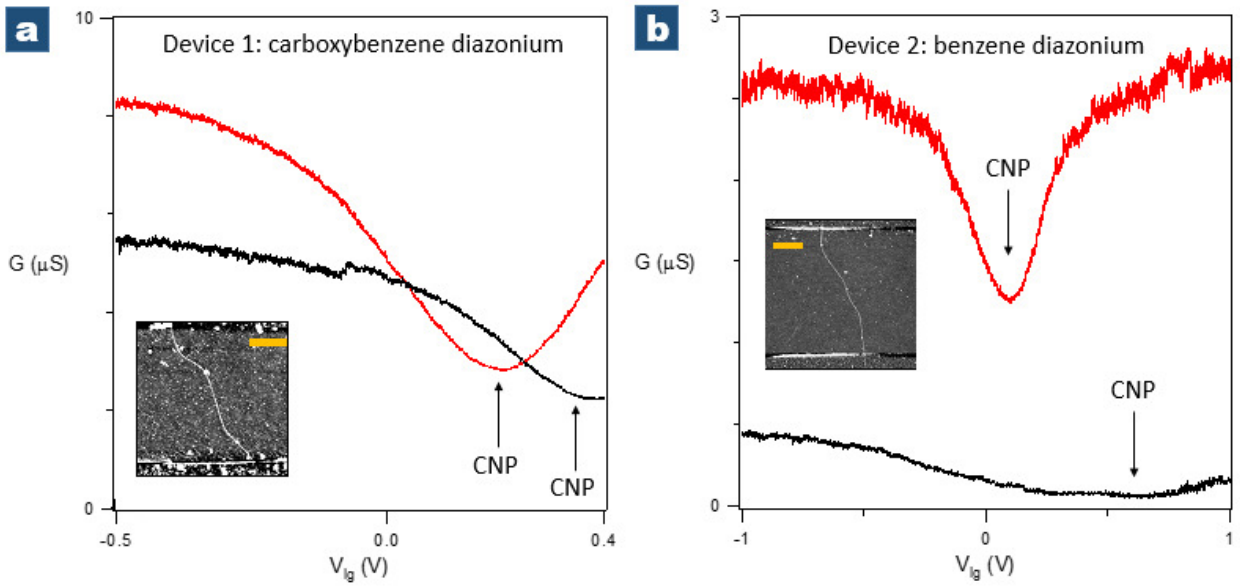

Figure 4.1. Electrical characteristics before and after a) 35 minute exposure to [CBD] = 0.75 mM on device 1 and b) a 20 minute exposure to [BD] = 7.5 mM on device 2. The approximate location of the charge neutrality point (CNP) is indicated. Insets display a topographical AFM image of the device's CNT, with electrode contacts above and below. The CNT diameter was 1.6 nm for device 1, and 2.5 nm for device 2 prior to diazonium exposure. Scale bars are 1 μm in length.

To investigate the uniformity of structural damage along the CNT, a scanning gold electrode was used to measure resistance as a function of CNT length. A complete circuit is formed between the CNTFET's drain electrode and a conductive AFM tip. A constant voltage bias was applied to the circuit as the AFM

tip scanned the CNT channel in tapping mode. The current at each point along the length of the CNT was measured.

Figure 4.2 shows the resistance measured between the left contact and AFM tip positioned a distance L along the CNT. As the CNT channel length L increases, a greater resistance is observed. For the undamaged CNT, the data points lie on a straight line with slope 8.2 kΩ μm^{-1} and y-intercept 84 kΩ. After damage, the data can be fit with a series of straight lines of approximate slope 16 kΩ μm^{-1} that are offset by jumps in resistance. The y-intercept increased to 222 kΩ.

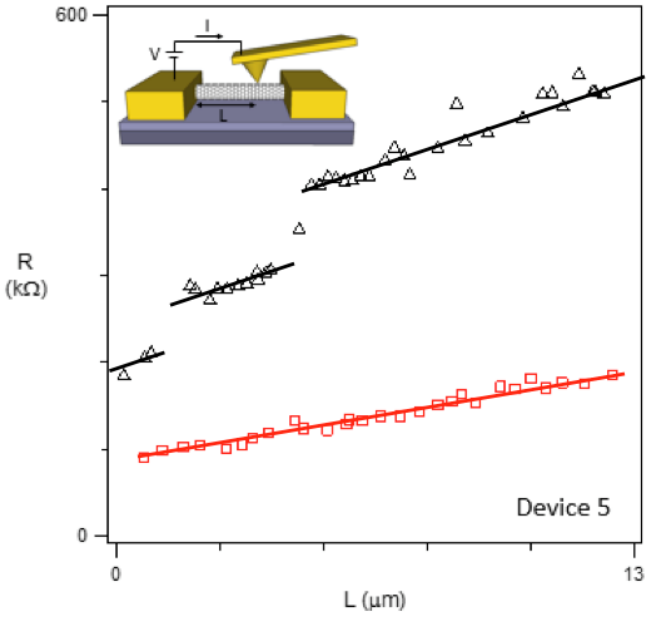

Figure 4.2. Resistance of device 5 as a function of channel length, before (squares) and after (triangles) exposure to carboxybenzene diazonium. The inset depicts the circuit diagram consisting of the CNT (length L), the gold coated AFM tip, and the metal electrode. The current conducted through this circuit was measured using a current-to-voltage preamplifier.

The conductance of the CNTFETs in this work were also monitored during the diazonium reaction. Figure 4.3 shows the resistance of a quasi-metallic CNT during CBD exposure. During the first 100 seconds, the increase in resistance with respect to time was approximately linear, with a slope of $dR/dt \approx 5$ kΩ s^{-1}. The rate slows down to $dR/dt \approx 2$ kΩ s^{-1}, and then drops to 0 kΩ s^{-1} at $t \approx 430$ s (not shown).

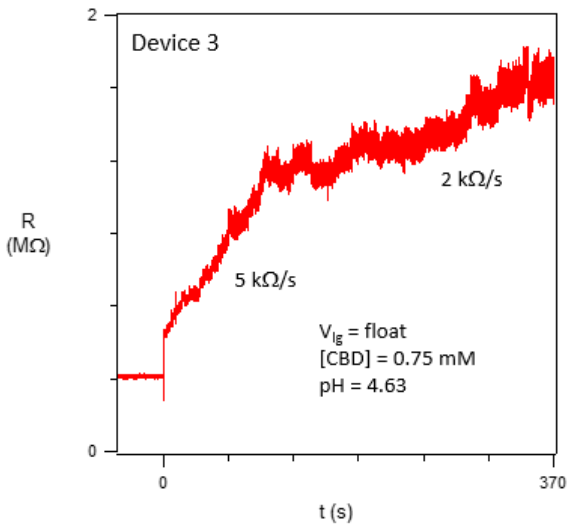

Figure 4.3. Change in resistance vs. time. V_{lg} was floating. [CBD] = 0.75 mM in 20 mM MES pH 4.63. Before t = 0, the CNT was exposed to buffer. After t = 0, the CNT was exposed to 0.75 mM CBD in buffer. The solution is not refreshed.

The effect of the liquid gate voltage, V_{lg}, on dR/dt was investigated for a semiconducting CNT, shown in Fig. 4.4. After introducing CBD, R(t) was recorded while varying V_{lg} between -0.2 V and +0.2 V as indicated. For each upward step in V_{lg}, there is an upward step in resistance (due to p-type charge carrier depletion). During the periods of constant V_{lg}, R(t) changes approximately linearly. A strong dependence of dR/dt on V_{lg} was observed. In Fig. 4.4a, dR/dt increased from 0.4 kΩ s^{-1} at V_{lg} = 0 mV to 2.5 kΩ s^{-1} at V_{lg} = +100 mV. In figure 4.4b at V_{lg} = - 50 mV (second segment), dR/dt starts at 0.4 kΩ s^{-1} and then drops to zero. Following an increase to V_{lg} = 0 (third segment), dR/dt returns to 0.4 kΩ s^{-1}. Similar behavior is observed over the 4^{th}, 5^{th} and 6^{th} segments: dR/dt was 0.7 kΩ s^{-1} at V_{lg} = +50 mV, but after decreasing V_{lg} 0 mV, dR/dt dropped to 0. Increasing V_{lg} back up to 100 mV restored dR/dt to 0.6 kΩ s^{-1}.

Table 4.1 lists the rates of change in resistance for various experimental parameters. It can be seen from this table that, in addition to liquid gate voltage, the magnitude of the source-drain bias and the chemical species involved also had an effect on dR/dt. Significantly larger values of V_{lg} and V_{sd} for BD relative to CBD were needed to yield a non-zero dR/dt. The effect of chemical concentration was inconclusive from this data set.

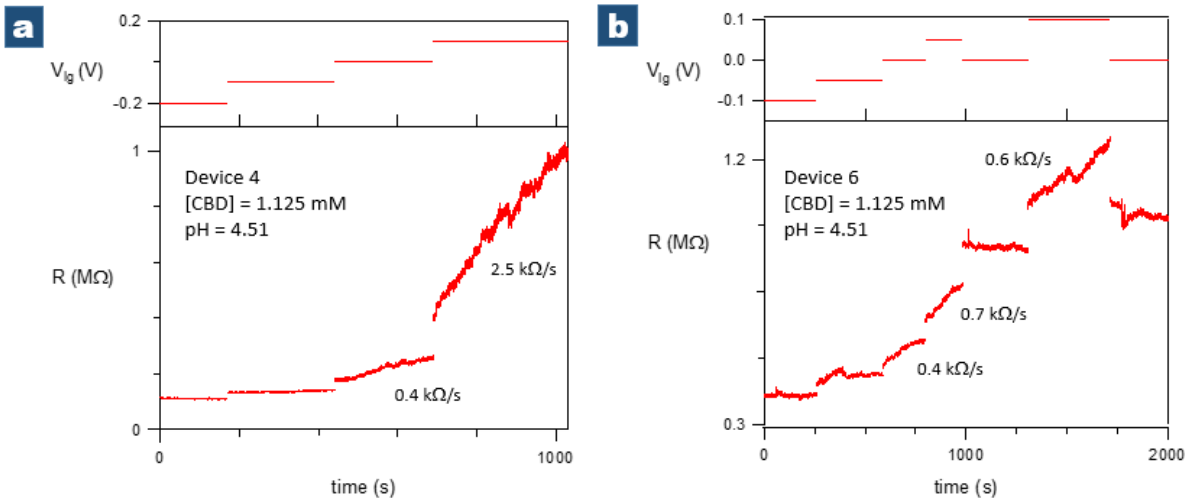

Figure 4.4. Applied liquid gate voltage, V_{lg}, with corresponding change in resistance as a function of time during exposure to 1.125 mM CBD on a) device 4 and b) device 6. The rate of resistance change, dR/dt, is given for selected segments.

species	concentration (mM)	V_{sd} (mV)	V_{lg} (mV)	dR/dt (kΩ s^{-1})
CBD	1.125	25	-200	0.0
CBD	0.75	25	-100	0.0
CBD	1.125	25	-100	0.0
CBD	1.432	25	0	0.0
CBD	0.75	25	0	0.0
BD	16.5	500	0	0.0
BD	0.75 & 16.5	500	float	0.0
CBD	1.125	25	0	0.1
CBD	0.75	25	100	0.1
CBD	0.75	25	200	0.1
CBD	1.125	25	-50	0.2
CBD	1.125	25	0	0.4
BD	16.5	500	300	0.5
CBD	1.125	25	50	0.7
CBD	1.432	25	100	0.7
CBD	1.125	25	100	1.8
BD	16.5	500	450	2.9
CBD	0.75	500	float	5.6
BD	7.5	500	200	15

Table 4.1. Chemical species, chemical concentration, source-drain bias, and liquid-gate voltage corresponding to rates of resistance increase dR/dt. In general, larger values of V_{lg} and V_{sd} result in larger dR/dt. The BD chemical species required larger values of V_{lg} and V_{sd} to yield non-zero rates. This table includes data from 6 experiments conducted at the same pH. Some of the data points in this table are averages of data with identical values in the first 4 columns. Data points where reaction was nearing completion were omitted.

In addition to the overall increase in R(t) during BD or CBD exposure, rapid (τ = 385 ± 170 μs) jumps in resistance were observed throughout the duration of the chemical reaction in all experiments conducted. Approximately an equal number of equal magnitude upward and downward discrete changes in resistance were observed. Prior to diazonium exposure, these discrete changes did not occur as shown in Fig. 4.5a. During diazonium exposure, Fig. 4.5b shows discrete resistance changes on the order of 10 kΩ. The size of these discrete changes increased with time (see Figure 4.5c).

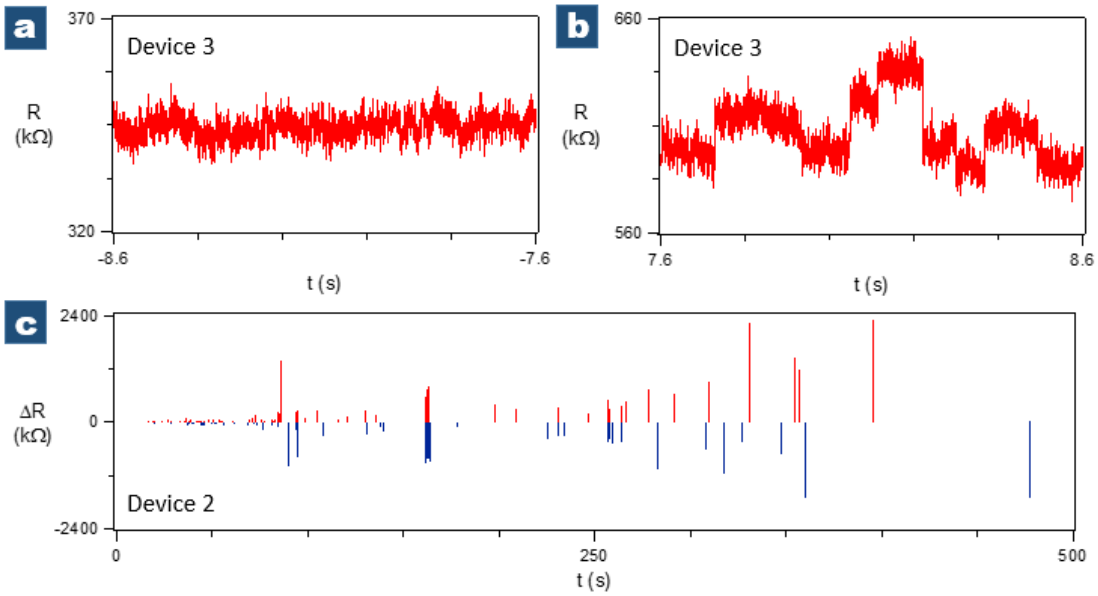

Figure 4.5. Resistance versus time for Device 3 a) in MES buffer at pH 4.63 prior to diazonium exposure. No rapid changes in resistance observed. b) During diazonium exposure, rapid, bidirectional changes in resistance were observed. R(t) data was collected at a rate of 6000 samples per second. c) Distribution of step sizes as a function of time for Device 2.

In summary, exposing CNTFET devices to BD or CBD decreased the conductivity of the devices and shifted the charge neutrality point to a more positive liquid gate voltage. Several factors affect the rate at which the resistance increases, including liquid gate voltage, source-drain voltage, and chemical species. Greater values of V_{lg} and V_{sd} increased dR/dt. The CBD species yields higher dR/dt than BD for lower values of V_{lg} and V_{sd}. Interestingly, an approximately equal number of upward and downward discrete changes in resistance occurred during diazonium exposure. In addition, CNTs had a larger diameter after diazonium exposure.

5. Discussion

The purpose of the diazonium experiments was to determine the suitability of carboxybenzene defects on CNTs for use in single-molecule biosensing experiments. Lattice defects are created when CBD (or BD) forms new sp^3 bonds on the CNT by breaking the existing sp^2 bonds in the CNT. Three major effects were observed as a result of this chemical reaction: i) a shift in the charge neutrality point, ii) a decrease in the overall conductance of the CNT, and iii) a decrease in slope of the transistor curve between the high and low conductance states. The latter two effects are of great concern because these may significantly lower the signal-to-noise ratio of single-molecule biosensing experiments. Fortunately, it was simultaneously discovered that the rate and extent of the diazonium-CNT reaction could be controlled and monitored.

The shift of the charge neutrality point (CNP) of graphene transistor curves after diazonium exposure has been previously explored and reported [29]. The electron from an unhybridized p_z orbital on a carbon atom in the CNT or graphene lattice is utilized in bond formation with an aryl radical. The new bond localizes the previously delocalized p_z electron, and transforms the p_z orbital into an sp^3 hybrid orbital. As a result of the localization, that electron can no longer participate in CNT conduction. This means that the aryl bond acts as an electron acceptor/p-type dopant. The hole-doping in the CNT manifests as a shift of the CNP in the transistor curve towards positive gate voltages.

The reduction of negative charge carrier concentration has a negligible contribution the total resistance of the CNTFET. The total CNTFET resistance after diazonium exposure can be described by the linear equation $R(L) = \rho L + R_c + R_h$. Figure 4.2 suggests that this increase in resistance can be attributed to an increase in resistivity ρ of the CNT, an increase in contact resistance R_c, and the presence of defect "hot-spots" R_h. The sharp changes in resistance in Fig. 4.2 evidence the presence of defect hot-spots R_h [30].

Figure 4.2 shows that the resistivity ρ of the CNT approximately doubles after diazonium exposure. This effect is primarily due to the new sp^3 bonds acting as point defects in the lattice. These defects scatter electrons and reduce the electrons' mean-free-path l, which is proportional to ρ. The presence of defects has also been shown to broaden the charge neutrality point in graphene due to uneven distribution of positive and negative charge carriers over the length of the CNT [31], [32]. We observe this charge carrier inhomogeneity as an increased shallowness of the transistor curve slope.

The increase in R_c indicates that the behavior of the CNT–electrode contact point is less Ohmic. The nature of the modification is unknown. It is possible that the aryl groups on the CNT near the contacts act as a very thin insulating layer. The charge transfer between CNT and metal would thus be subject to a potential barrier, and the contact point would act as a tunnel junction. The electrons would only be able to pass through this barrier by quantum mechanical tunneling. Another possibility is that the contact points behave as Schottky barriers, since the contacts consist of a metal and a semiconductor. The height of a Schottky barrier is the difference in energy between the Fermi level of the metal and the valence band of a p-type semiconductor or conduction band of an n-type semiconductor. The Schottky barrier height between the CNT and metal may have increased after diazonium exposure, perhaps due to a decrease in the valence band energy of the CNT.

The increase in contact resistance may decrease the range of the magnitude of the signal that can be transduced in biosensing experiments, due to the shortening of the sub-threshold region of the transistor curve. In addition, the presence of sp^3 lattice defects may decrease the signal-to-noise ratio, depending on what the single-molecule sensing mechanism is. The signal transduction mechanism is still under debate. Collins proposes that surface charges on the molecule have an electrostatic-gating effect, and Minot suggests that the surface charges may instead behave as a potential well or barrier (see section 2.2.2). If the gating mechanism is applicable, then the signals observed with devices heavily damaged by CBD will be smaller because the transistor curve's slope is reduced. For both mechanisms, the presence of excess carboxybenzene groups on the CNT's surface may electrostatically shield the single-molecule surface charges, reducing the magnitude of the signal from the molecule.

In an effort to determine if the extent of the CBD-CNT reaction could be controlled, various experimental parameters were manipulated. Figure 4.3 shows that R(t) was initially linear, suggesting that dR/dt can be used as a rough measure of dN/dt, where N is the number of aryl groups bound to the CNT. The association between dR/dt and dN/dt is consistent with the theoretical description of diffusive transport through a series of scattering sites in a 1d conductor [14].

It was found that the liquid gate voltage and source-drain bias could be used to control the rate dN/dt and extent of carboxybenzene defect creation on the CNT. The cation of the CBD salt (positively charged component) must first undergo reduction (i.e. gain an electron) prior to reaction with the CNT. The reduction of the cation can be accomplished by application of a negative potential to the reaction solution [23], [33]. In these experiments, applying a positive potential to the solution means the CNT channel has a negative potential relative to the solution, and thus cation reduction is achieved in the

vicinity of the CNT. The source-drain bias has a similar effect since one electrode has a negative potential relative to the other. Applying a positive V_{lg} increases the Fermi level of the CNT, thus increasing the availability of p_z electrons for charge transfer to the diazonium cation [22]. However, an unlimited supply of electrons is also available for diazonium reduction at the source-drain electrodes.

It was observed that when V_{lg} is held constant, the reaction rate slows down and then ceases as evidenced by the decrease in dR/dt illustrated in Fig. 4.3 as well as the second segment of Fig. 4.4b. However, increasing V_{lg} often increases dR/dt from zero to a non-zero value as shown in Fig 4.4b, indicating that the reaction can been re-initiated. The slowing of the chemical reaction can be explained by pointing out that, as the chemical reaction progresses, the charge neutrality point slowly shifts towards positive gate voltages. The Fermi level ε_F decreases while V_{lg} is held constant as a result. Although electrons from the source-drain electrodes can reduce the diazonium cations to aryl radicals, it makes sense that the majority of the aryl radicals bonding with the CNT are formed at the surface of the CNT due to proximity. The reduction occurs by electron transfer from a p_z electron on the CNT, and that electron is then quickly replaced by an electron from the source or drain electrode. Increasing V_{lg} then increases the Fermi level, and thus the reaction rate.

After the highly reactive aryl radical is formed by reduction of the diazonium cation, the radical then forms a bond with the CNT. This causes the CNT to become a radical itself. The role and effect of the new CNT radical has been explored theoretically [28], and may explain the discrete changes in resistance observed during diazonium exposure (see Fig. 4.5). It was theoretically determined that there is some probability that the radical electron may cause the new aryl bond to break in favor of reformation of the sp^2 bond. Isolated aryl groups on small diameter CNTs (d = 1 nm) are relatively stable (rate constant $k \approx 10^{-3}\ s^{-1}$), while isolated benzene groups on graphene are quite unstable ($k \approx 10^{3}\ s^{-1}$) [28]. The CNTs in this work range in diameter from d = 1.5 nm to 2.9 nm, thus a rate constant of $10^{-3} < k < 10^{3}\ s^{-1}$ was expected. The discrete changes in resistance in these experiments all occur within this timescale range.

The desorption of carboxybenzene groups seems to be an unlikely explanation for the discrete resistance changes in light of the observation that approximately equal numbers of upward and downward steps occurred. A more plausible explanation for the discrete changes in dR/dt is that the chemical potential μ in the CNT shifts during the reaction, and the new chemical potential becomes resonant with a charge trap in the SiO_2. In this context, a charge trap is a location on the SiO_2 near the CNT that has an affinity for electrons. The charge trap is referred to as resonant with the CNT when the energy of the electron is similar at both locations. If the charge trap is resonant with the CNT, an

electron can jump from the CNT to the trap, and back again. While the electron is in the trap, it can interact with the CNT by the mechanisms discussed for single-molecule biosensing.

In regards to Table 4.1, it is obvious that the trends in dR/dt lack consistency. For example, dR/dt for BD at V_{lg} = 450 mV was five times less than dR/dt for BD at V_{lg} = 200 mV. Table 4.1 includes data from several experiments. When looking within individual experiments, the correlation between dR/dt and V_{lg} was much clearer (see Fig. 4.4 for example). There are several possible explanations for the variations between experiments.

One possible explanation is that diazonium reagents have been shown to be more reactive towards metallic CNTs than semiconducting CNTs [22]. The chiralities of the CNTs used in these experiments were unknown. It is also widely accepted that smaller diameter CNTs are more chemically reactive than larger diameter CNTs due to curvature strain [34]. There is insufficient data to compare the effect of CNT diameter on reaction rate in this set of experiments.

6. Conclusions

The primary goal of this project was to assist in the development of single-molecule biosensing using CNTFETs. Initial attempts at repeating Collins' published experimental work proved to be much more challenging than anticipated. In an effort to determine if other bioconjugation methods might be more practical, carboxybenzene diazonium was investigated as a precursor for linking enzymes to CNTs in CNTFETs. The electrical properties of the CNTFET were compared before, during and after exposure of devices to CBD.

We found that excessive CBD exposure tends to inhibit some of the properties that make CNTFETs so desirable for single-molecule biosensing. However, we also found that the extent of the reaction could be monitored and controlled in real-time. Since only single-enzyme attachments are desired for these devices, minimal carboxybenzene functionalization of the CNT is needed. We conclude that CBD functionalization of CNTFETs may be a plausible route to bioconjugation.

In future work, CNTFET devices can be minimally functionalized with carboxybenzene groups using the methods of reaction rate monitoring described in this work. Further experiments can be done to test the ease at which enzymes can be attached to the functionalized CNTs, and comparison could be made to the pyrene maleimide method used by Collins. In light of the debate regarding the mechanism involved in enzyme signal transduction, computational studies may also be useful in predicting how enzyme kinetics affect the conductance of a CNTFET.

7. Acknowledgements

This work was financially supported by the Undergraduate Research, Innovation, Scholarship and Creativity (URISC) grant and the Human Frontier Science Program (HFSP) grant. I thank my thesis advisor Professor Ethan Minot for direction, guidance and support in this project. I acknowledge Professor Daniel Myles for supplying the diazonium reagents used in this work, and Professor Ryan Mehl for supplying lysozyme proteins and helpful advice. I thank Professor Kerstin Blank and graduate student Sophie Ripp for valuable discussions and guidance. I appreciate many valuable discussions, extensive training, and protocol development from Dr. Landon Prisbrey. I also acknowledge helpful discussions and instruction from graduate student Tal Sharf, Dr. Tristan DeBorde, and Professor Aleksandra Sikora.

8. References

[1] J. A. Hanson, K. Duderstadt, L. P. Watkins, S. Bhattacharyya, J. Brokaw, J.-W. Chu, and H. Yang, "Illuminating the mechanistic roles of enzyme conformational dynamics," *PNAS*, vol. 104, no. 46, pp. 18055–18060, Nov. 2007.

[2] K. A. Henzler-Wildman, V. Thai, M. Lei, M. Ott, M. Wolf-Watz, T. Fenn, E. Pozharski, M. A. Wilson, G. A. Petsko, M. Karplus, C. G. Hübner, and D. Kern, "Intrinsic motions along an enzymatic reaction trajectory," *Nature*, vol. 450, no. 7171, pp. 838–844, Dec. 2007.

[3] Y. Choi, G. A. Weiss, and P. G. Collins, "Single molecule recordings of lysozyme activity," *Phys. Chem. Chem. Phys.*, vol. 15, no. 36, pp. 14879–14895, Aug. 2013.

[4] T. Sharf, J. W. Kevek, T. DeBorde, J. L. Wardini, and E. D. Minot, "Origins of Charge Noise in Carbon Nanotube Field-Effect Transistor Biosensors," *Nano Lett.*, vol. 12, no. 12, pp. 6380–6384, Dec. 2012.

[5] M. B. Lerner, J. M. Resczenski, A. Amin, R. R. Johnson, J. I. Goldsmith, and A. T. C. Johnson, "Toward Quantifying the Electrostatic Transduction Mechanism in Carbon Nanotube Molecular Sensors," *J. Am. Chem. Soc.*, vol. 134, no. 35, pp. 14318–14321, Sep. 2012.

[6] Y. Choi, T. J. Olsen, P. C. Sims, I. S. Moody, B. L. Corso, M. N. Dang, G. A. Weiss, and P. G. Collins, "Dissecting Single-Molecule Signal Transduction in Carbon Nanotube Circuits with Protein Engineering," *Nano Lett.*, vol. 13, no. 2, pp. 625–631, Feb. 2013.

[7] T. J. Olsen, Y. Choi, P. C. Sims, O. T. Gul, B. L. Corso, C. Dong, W. A. Brown, P. G. Collins, and G. A. Weiss, "Electronic Measurements of Single-Molecule Processing by DNA Polymerase I (Klenow Fragment)," *J. Am. Chem. Soc.*, vol. 135, no. 21, pp. 7855–7860, May 2013.

[8] P. C. Sims, I. S. Moody, Y. Choi, C. Dong, M. Iftikhar, B. L. Corso, O. T. Gul, P. G. Collins, and G. A. Weiss, "Electronic Measurements of Single-Molecule Catalysis by cAMP-Dependent Protein Kinase A," *J. Am. Chem. Soc.*, vol. 135, no. 21, pp. 7861–7868, May 2013.

[9] Y. Choi, I. S. Moody, P. C. Sims, S. R. Hunt, B. L. Corso, I. Perez, G. A. Weiss, and P. G. Collins, "Single-Molecule Lysozyme Dynamics Monitored by an Electronic Circuit," *Science*, vol. 335, no. 6066, pp. 319–324, Jan. 2012.

[10] Y. Choi, I. S. Moody, P. C. Sims, S. R. Hunt, B. L. Corso, D. E. Seitz, L. C. Blaszczak, P. G. Collins, and G. A. Weiss, "Single-Molecule Dynamics of Lysozyme Processing Distinguishes Linear and Cross-Linked Peptidoglycan Substrates," *J. Am. Chem. Soc.*, vol. 134, no. 4, pp. 2032–2035, Feb. 2012.

[11] M. Scarselli, P. Castrucci, and M. De Crescenzi, "Electronic and optoelectronic nano-devices based on carbon nanotubes," *Journal of Physics: Condensed Matter*, vol. 24, no. 31, p. 313202, Aug. 2012.

[12] C. Zhou, J. Kong, and H. Dai, "Intrinsic Electrical Properties of Individual Single-Walled Carbon Nanotubes with Small Band Gaps," *Phys. Rev. Lett.*, vol. 84, no. 24, pp. 5604–5607, Jun. 2000.

[13] M. S. Purewal, B. H. Hong, A. Ravi, B. Chandra, J. Hone, and P. Kim, "Scaling of Resistance and Electron Mean Free Path of Single-Walled Carbon Nanotubes," *Phys. Rev. Lett.*, vol. 98, no. 18, p. 186808, May 2007.

[14] C. Kittel, *Introduction to Solid State Physics*, 8th ed. John Wiley & Sons, Inc, 2005.

[15] H. J. Choi, J. Ihm, S. G. Louie, and M. L. Cohen, "Defects, Quasibound States, and Quantum Conductance in Metallic Carbon Nanotubes," *Phys. Rev. Lett.*, vol. 84, no. 13, pp. 2917–2920, Mar. 2000.

[16] N.-P. Wang, S. Heinze, and J. Tersoff, "Random-Telegraph-Signal Noise and Device Variability in Ballistic Nanotube Transistors," *Nano Lett.*, vol. 7, no. 4, pp. 910–913, Apr. 2007.

[17] J. L. Bahr and J. M. Tour, "Highly Functionalized Carbon Nanotubes Using in Situ Generated Diazonium Compounds," *Chem. Mater.*, vol. 13, no. 11, pp. 3823–3824, Nov. 2001.

[18] Y. Gao and I. Kyratzis, “Covalent Immobilization of Proteins on Carbon Nanotubes Using the Cross-Linker 1-Ethyl-3-(3-dimethylaminopropyl)carbodiimide—a Critical Assessment,” *Bioconjugate Chem.*, vol. 19, no. 10, pp. 1945–1950, Oct. 2008.
[19] K. Jiang, L. S. Schadler, R. W. Siegel, X. Zhang, H. Zhang, and M. Terrones, “Protein immobilization on carbon nanotubes via a two-step process of diimide-activated amidation,” *J. Mater. Chem.*, vol. 14, no. 1, pp. 37–39, Dec. 2004.
[20] A. López-Bezanilla, F. Triozon, S. Latil, X. Blase, and S. Roche, “Effect of the Chemical Functionalization on Charge Transport in Carbon Nanotubes at the Mesoscopic Scale,” *Nano Lett.*, vol. 9, no. 3, pp. 940–944, Mar. 2009.
[21] A. Lopez-Bezanilla, “Electronic Transport Properties of Chemically Modified Double-Walled Carbon Nanotubes,” *J. Phys. Chem. C*, vol. 117, no. 29, pp. 15266–15271, Jul. 2013.
[22] M. S. Strano, C. A. Dyke, M. L. Usrey, P. W. Barone, M. J. Allen, H. Shan, C. Kittrell, R. H. Hauge, J. M. Tour, and R. E. Smalley, “Electronic Structure Control of Single-Walled Carbon Nanotube Functionalization,” *Science*, vol. 301, no. 5639, pp. 1519–1522, Sep. 2003.
[23] J. L. Bahr, J. Yang, D. V. Kosynkin, M. J. Bronikowski, R. E. Smalley, and J. M. Tour, “Functionalization of Carbon Nanotubes by Electrochemical Reduction of Aryl Diazonium Salts: A Bucky Paper Electrode,” *J. Am. Chem. Soc.*, vol. 123, no. 27, pp. 6536–6542, Jul. 2001.
[24] C. A. Dyke, M. P. Stewart, F. Maya, and J. M. Tour, “Diazonium-Based Functionalization of Carbon Nanotubes: XPS and GC-MS Analysis and Mechanistic Implications,” *Synlett*, no. 1, pp. 155–160, 2004.
[25] A. J. Hilmer, T. P. McNicholas, S. Lin, J. Zhang, Q. H. Wang, J. D. Mendenhall, C. Song, D. A. Heller, P. W. Barone, D. Blankschtein, and M. S. Strano, “Role of Adsorbed Surfactant in the Reaction of Aryl Diazonium Salts with Single-Walled Carbon Nanotubes,” *Langmuir*, vol. 28, no. 2, pp. 1309–1321, Jan. 2012.
[26] G. Schmidt, S. Gallon, S. Esnouf, J.-P. Bourgoin, and P. Chenevier, “Mechanism of the Coupling of Diazonium to Single-Walled Carbon Nanotubes and Its Consequences,” *Chem. Eur. J.*, vol. 15, no. 9, pp. 2101–2110, Feb. 2009.
[27] J. G. Smith, *Organic Chemistry*, 3rd ed. McGraw-Hill, 2011.
[28] E. R. Margine, M.-L. Bocquet, and X. Blase, “Thermal Stability of Graphene and Nanotube Covalent Functionalization,” *Nano Lett.*, vol. 8, no. 10, pp. 3315–3319, Oct. 2008.
[29] X.-Y. Fan, R. Nouchi, L.-C. Yin, and K. Tanigaki, “Effects of electron-transfer chemical modification on the electrical characteristics of graphene,” *Nanotechnology*, vol. 21, no. 47, p. 475208, Nov. 2010.
[30] J.-Y. Park, “Electrically tunable defects in metallic single-walled carbon nanotubes,” *Applied Physics Letters*, vol. 90, no. 2, p. 023112, Jan. 2007.
[31] J. Martin, N. Akerman, G. Ulbricht, T. Lohmann, J. H. Smet, K. von Klitzing, and A. Yacoby, “Observation of electron–hole puddles in graphene using a scanning single-electron transistor,” *Nat Phys*, vol. 4, no. 2, pp. 144–148, Feb. 2008.
[32] E. H. Hwang, S. Adam, and S. Das Sarma, “Carrier Transport in Two-Dimensional Graphene Layers,” *Phys. Rev. Lett.*, vol. 98, no. 18, p. 186806, May 2007.
[33] M. Knez, M. Sumser, A. M. Bittner, C. Wege, H. Jeske, S. Kooi, M. Burghard, and K. Kern, “Electrochemical modification of individual nano-objects,” *Journal of Electroanalytical Chemistry*, vol. 522, no. 1, pp. 70–74, Mar. 2002.
[34] R. C. Haddon, “Chemistry of the Fullerenes: The Manifestation of Strain in a Class of Continuous Aromatic Molecules,” *Science*, vol. 261, no. 5128, pp. 1545–1550, Sep. 1993.